energies

MDPI

Article

Electromagnetic Analysis of Double-Rotor Direct-Drive Permanent Magnet Generators Under Eccentricity Faults

Marios Salinas [1], Alexandros Sergakis [1], Markus Mueller [2] and Konstantinos N. Gyftakis [1,*]

[1] School of Electrical and Computer Engineering, Technical University of Crete, 731 00 Chania, Greece; msalinas@tuc.gr (M.S.); asergakis1@tuc.gr (A.S.)
[2] School of Engineering, University of Edinburgh, Edinburgh EH9 3FB, UK; markus.mueller@ed.ac.uk
* Correspondence: k.n.gyftakis@ieee.org

Abstract

Permanent Magnet Synchronous Generators (PMSGs) have acquired a pivotal role in recent years, owing to their high-power density, high efficiency, and ability to operate in direct-drive configurations. Despite these advantages, such machines are susceptible to mechanical faults, particularly airgap eccentricity, with axial flux topologies being more vulnerable due to their high ratio of axial to radial length. Given the rapidly increasing deployment rates of these generators, this paper focuses on the electromagnetic analysis of a coreless axial flux dual-rotor direct-drive PMSG, with the analysis focusing on eccentricity faults. Static (SE) and dynamic (DE) eccentricities are investigated under a specific load condition using 3D finite element analysis (FEA) models. For the investigation of the fault scenarios, this work utilizes traditional signature analysis methods, namely Current Fast Fourier Transform (FFT), Voltage FFT, and Electromagnetic Torque Analysis.

Keywords: permanent magnet synchronous generators; condition monitoring; fault diagnosis; eccentricity; electromagnetic analysis

1. Introduction

The utilization of PMSGs in renewable energy systems for wave, tidal, and wind energy harvesting has been significantly rising throughout the years, as a result of their high torque density, small relative size, low weight, and reduced maintenance requirements [1,2]. One of the machines that has gained attention in these applications is the C-GEN coreless axial flux PMSG, which was developed at the University of Edinburgh. This topology is a lightweight and scalable PMSG with modular C-shaped back-iron segments and surface-mounted permanent magnets (PMs) [3]. The modular architecture is advantageous for offshore or remote installations, where maintenance interventions are challenging due to limited accessibility and high operational costs, as individual faulty modules can be identified and replaced independently without dismantling the entire generator. The coreless structure can help reduce the cogging torque and unwanted magnetic attraction forces, making the generator highly effective and reliable [4]. Additionally, owing to the high number of magnetic pole pairs and the large effective diameter, the generator delivers high torque at low mechanical speeds, making it ideal for direct-drive applications [5,6]. However, the axial flux PMSGs are prone to mechanical faults that can deteriorate performance and reliability over time. The large diameter and relatively small axial length of these generators result in reduced structural stiffness and increased sensitivity to shaft deflection, bearing degradation, and assembly misalignment, increasing the probability of eccentricity

Academic Editor: Lorand Szabo

Received: 24 January 2026
Revised: 17 February 2026
Accepted: 20 February 2026
Published: 22 February 2026

faults during operation [7]. Additionally, in renewable energy applications, these machines are frequently subjected to variable torque loading, uneven mechanical stresses, as well as environmental factors such as humidity and corrosion, which can also accelerate the appearance of eccentricity or worsen its severity. Furthermore, the small airgap length of the axial flux topologies, along with the strong magnetic pull that is present due to the PMs, makes these topologies highly sensitive to even minor deviations, meaning that small mechanical displacements can lead to significant eccentricity-related effects.

Eccentricity is often the most common consequence of mechanical deterioration, as it results from several underlying mechanical issues [8]. This defect can be present as SE, DE, or a combination of both, ME. Typically, SE originates from the manufacturing stage due to assembly errors. This is a frequent fault that appears in a low severity percentage, even before the machine starts its first operation. For that reason, an acceptable tolerance limit is defined, and machines must remain within this limit before being released [9]. On the other hand, DE is the result of mechanical degradation and grows during the operation. The time-varying nature of this fault results in stronger spectral modulation, making it easier to detect. Addressing these faults is of critical importance as even small deviations in rotor alignment or mechanical loading distort the airgap geometry and consequently the electromagnetic field distribution [10]. If left unaddressed, such faults will lead to increased torque ripples, vibrations, component wear, and eventually a reduced lifespan [11,12]. For that reason, extensive research has been carried out to detect eccentricity by utilizing commonly used methods and modern approaches.

Most of the techniques are based on monitoring the stator current and voltage. Stator current FFT analysis is a well-known and widely adopted method, owing to its non-intrusive nature and suitability for online condition monitoring. In PMSGs, several works utilize this method in order to detect eccentricity faults as well as demagnetization by tracking the fault frequency components [13–16]. Recent diagnostic frameworks also integrate FFT-based current features to enhance detection and classification performance for PMSG faults [17]. Another impressive work suggests the use of current analysis by utilizing a multi-stage framework [18]. This study combines FEA-based current synthesis, wavelet-based feature extraction, autoregressive modeling, principal component analysis, and fuzzy SVM classification to identify the eccentricity type and severity with high accuracy. As previously mentioned, stator voltage signals have also been leveraged for eccentricity detection in PMSGs. For instance, a study has used the stator voltage signature analysis to identify distinctive frequency components associated with SE, DE, and ME in a PMSG [19,20]. Other works examine the zero-sequence voltage components (ZSVCs), since mechanical misalignments introduce asymmetries that are reflected in the voltage spectra, offering a richer spectrum than that of the current [21]. In a recent work based on axial flux PMSGs, the author demonstrated that applying FFT to the neutral point voltage difference signals yields new harmonics under different eccentric conditions and provides clear indications of the presence of SE and demagnetization [22]. These studies confirm that both voltage- and current-related features can serve as effective indicators for detecting eccentricity, especially when the analysis is based on the combination of both.

The electromagnetic torque has also been investigated as a valid diagnostic indicator of eccentricity. An eccentric rotor produces characteristic torque ripple patterns, making both the spectral and time signal analysis of the torque a valuable tool. A good example is a study that focused on a PMSG used in wave energy harvesting applications, which reported that even a slight percentage of SE caused a ~58% rise in torque ripple amplitude and introduced noticeable radial harmonic components in the torque FFT spectrum, namely the eighth and sixth harmonic components [23]. The SE effect on torque has also been studied by comparing single-sided and double-sided rotor topologies [24]. It was concluded that

double-rotor topologies are more resistant to SE defects, as only the single-rotor topology showed a significant increase in space harmonics.

Despite extensive research on eccentricity fault detection in conventional PMSGs, there is still a significant research gap concerning coreless as well as axial double-rotor topologies. The absence of an iron core leads to the creation of non-guided flux paths in the airgap and a lower overall airgap flux density that may alter the expression of fault harmonics. Additionally, the symmetrical nature of double-rotor configurations may cause mutual cancelation of asymmetries, with the highest impact being observed for static faults. For those reasons, this investigation aims for an electromagnetic analysis and fault signature identification in a coreless dual-rotor axial flux C-GEN PMSG in order to assess the impact of this advanced topology on the appearance of the fault signatures. The investigation consists of studying SE and DE applied through different mechanical offset conditions, namely radial, axial, and angular offsets. The analysis is conducted using 3D FEA models, evaluating the impact on the stator current and voltage spectrum and the electromagnetic torque characteristics.

The structure of this paper is organized as follows. Section 2 presents the development of the 3D model, consisting of the input parameters used to calibrate the model, the signal acquisition method, and the accuracy assessment of the model with the experimental data. In Section 3, the eccentricity configurations are defined along with the spatial offset modes, and the diagnostic results of each case are presented. Finally, the last section summarizes the main findings and indicates future directions.

2. Model Development

The geometric complexity of the studied topology required a 3D FEA model for the accurate acquisition of the simulation results. The simulation was carried out using magnetostatic analysis software Simcenter Magnet with a fully transient 3D rotational motion solver. The sampling frequency used for the solver is 1 kHz, which corresponds to a time-step of 1 ms, and the total simulation time is 3.2 s. Given the generator's speed input of 80 rpms and the 24 pole pairs, the total simulation time consisted of 4.26 mechanical periods or 102.24 electrical periods. For the purpose of generating the FFT spectra of the electromagnetic quantities, the first 200 ms of the simulation results were discarded to eliminate any minor start-up transients. Therefore, the FFT analysis was conducted using the subsequent four complete mechanical rotation periods using a Hanning window function to minimize spectral leakage, and the resulting spectra were amplitude-normalized with respect to the fundamental harmonic of each case for consistent comparison.

The parameterization of the model was conducted by defining the generator geometry, material properties, winding layout, and operating conditions. Additionally, in order to enhance the accuracy of the magnetostatic solutions, a finer mesh was applied in the airgap regions, where magnetic field variations are most critical. The generator is connected in a star configuration with phase resistances of 18.5 Ω, and the stator coils of each phase are connected in series. In Figures 1 and 2, the healthy model of the PMSG is showcased, as well as the magnetic field distribution. The nominal characteristics of the generator are given in Table 1. Finally, Table 2 presents a comparison between the FEA simulation results and experimental measurements, demonstrating a low deviation between them. The measurements were obtained at 80 rpm with a three-phase resistive load of 18.5 Ω per phase, under the same operating conditions used in the FEA model. This close agreement validates the model's accuracy for diagnostic purposes.

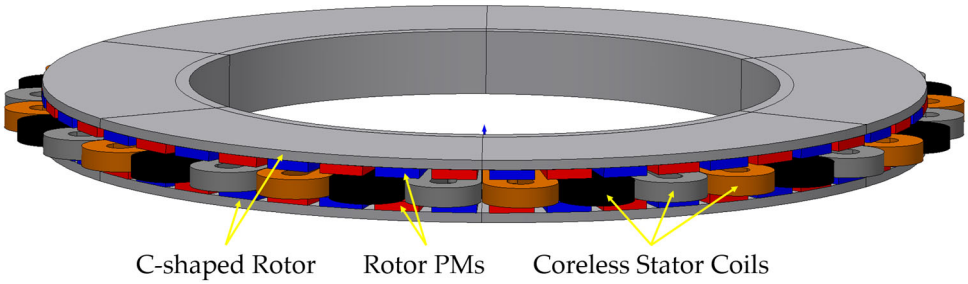

Figure 1. 3D sectional isometric view of the coreless double-rotor axial flux PMSG.

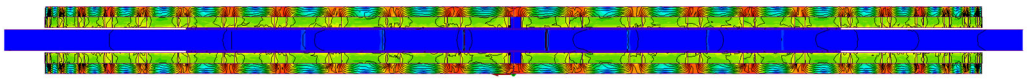

Figure 2. Magnetic field representation of the 3D FEA model.

Table 1. Nominal characteristics of the studied generator.

Characteristic	Value
Rated power (kW)	8
Rated speed (rpm)	80
Frequency (Hz)	32
Pole pairs	24
Number of stator coils	36
Coil type	Single concentrated
Number of coil turns	90
PM type	N42

Table 2. Accuracy assessment of the 3D FEA model [25].

	FEA	Experimental	Deviation (%)
Phase Voltage (V)	222.4	217.5	2.25
Phase Current (A)	12.02	12.4	3.06
Torque (Nm)	1145.5	1067	7.35
Electrical Power (kW)	8.02	8.06	0.49
Mechanical Power (kW)	9.5	8.93	6.38
Efficiency (%)	85.3	90.28	5.51

3. Eccentricity Faults

The SE fault occurs when the geometrical axis of the rotor is displaced relative to the geometrical axis of the stator but maintains a stable rotational axis. In contrast, the DE fault is a condition where the rotor rotational axis is not fixed in space; therefore, it produces an uneven airgap that revolves with the rotor. Whether eccentricity is static (SE) or dynamic (DE), it affects how easily it can be detected. In practice, both types often occur together, especially in machines that have been in operation for a long time, a type which is called ME. In Figure 3, a comparative diagram showcases the various types of eccentricities using radial flux models, which clearly depict the relationship between the rotor center, the stator center, and the rotational center [26]. Following a similar theoretical framework, the same principles apply to axial flux machines, which are the focus of this study.

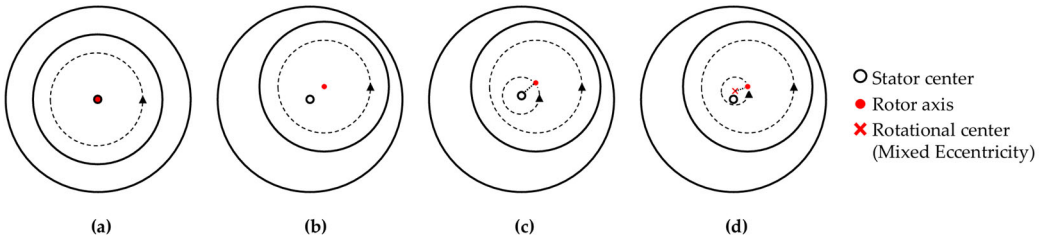

Figure 3. Representation of machine conditions: (**a**) healthy configuration, (**b**) SE, (**c**) DE, and (**d**) ME fault scenarios.

In double-rotor axial flux machines, eccentricity can manifest in multiple spatial configurations depending on the direction of the rotor displacement. Axial offset eccentricity occurs when the rotor is laterally displaced through the axis of rotation, leading to a reduced airgap length on one side of the stator and an increased airgap on the opposite side. This type of offset can only be present in SE conditions due to the nature of the topology. Radial offset occurs when the rotor shifts along the radial direction of the machine, leading to a non-uniform airgap across the stator's circumference. Angular offset (or inclined) eccentricity is more common than the other two configurations in disk-shaped machines. This configuration refers to a tilt in the rotor relative to the stator plane, causing the airgap to vary across the radial direction of the machine. Each of these eccentricity configurations induces different patterns of magnetic field distortion, and for that reason, this study evaluates the impact of each individually. Figure 4 illustrates the previously discussed eccentricity configurations, where g_0 is the airgap length in the healthy case, g_{min} and g_{max} are the minimum and maximum airgap lengths, Δr is the radial displacement, and β is the deviation angle. Each case is represented by a simplified cross-section of the machine, showing the stator coil and the c-shaped back iron, to clearly show the direction of displacement. It is important to note that the stator is treated as a rigid body in all configurations, meaning that the entire stator is uniformly displaced.

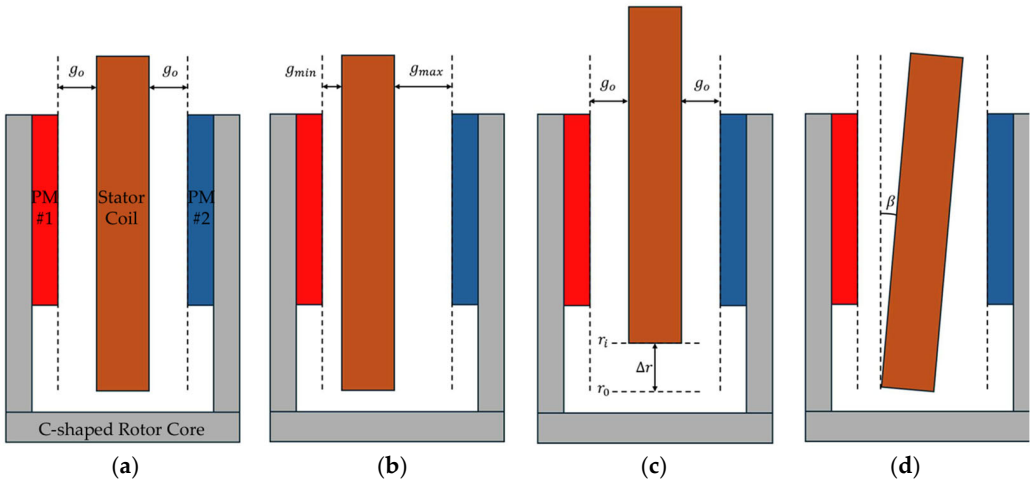

Figure 4. Cross-sectional view of the studied c-shaped coreless double-rotor axial flux PMSG for the healthy and eccentric topologies (**a**) healthy, (**b**) axial offset, (**c**) radial offset, and (**d**) angular offset.

3.1. Static Eccentricity

The SE fault was studied by utilizing all the previously discussed configurations. The severity assessment of the radial offset case was conducted in a different manner, as the fault ratio is quantified as the radial displacement Δr, calculated as the difference between the stator coil's final position r_i after the offset and its original position r_0. The radial offset eccentricity alters the airgap permeance not by changing the airgap length directly but by

displacing the stator coils radially. This causes the primary flux paths between the rotor PMs and the stator windings to exhibit increased permeance in specific regions, which leads to the asymmetry being present. The radial offset introduced in this study is 1.64 mm. For axial offset, fault severity was defined as the total axial displacement relative to the rotor airgap length, with a severity level of 40%. The angular offset severity was assessed as the ratio of the lateral displacement and the airgap length [27]. The deviation angle that was introduced is 0.1°, which corresponds to a severity level of 40%.

3.1.1. Current FFT Analysis

Static faults typically lead to the amplification of harmonic components that are odd multiples of the fundamental electrical frequency (f_s). This phenomenon is the result of the asymmetry being fixed in space, while the rotor's permanent magnets, which generate the dominant magnetic poles, rotate past the affected regions, which makes the stator windings experience a periodic disturbance once per electrical cycle. However, in the case of a coreless dual-rotor design, the asymmetry is mirrored between the two rotors, which results in the cancelation of the fault-related harmonics [28]. Recent studies have confirmed this mirroring phenomenon in coreless dual-rotor axial machines by evaluating the unbalanced magnetic pull, demonstrating that opposing axial force components induced by the two rotor disks counteract each other, resulting in a cancellation of the asymmetry effects that could be induced in the current stator under SE conditions [29]. Furthermore, the absence of a ferromagnetic core prevents the induction of spatial magnetic field asymmetries. Hence, the effectiveness of the current-based analysis in detecting SE is significantly reduced. The corresponding FFT results for the SE cases are presented in Table 3 and Figure 5, where minimal amplitude differences can be observed between the healthy and faulty cases.

Table 3. Amplitudes of the 3rd, 5th, and 7th harmonics in the current spectrum for each SE type compared to the healthy case.

Case	$3f_s$ (dB)	$5f_s$ (dB)	$7f_s$ (dB)
Healthy	−79.54	−82.97	−85.7
Axial offset (40%)	−82.57	−82.65	−86.19
Radial offset (1.64 mm)	−79.47	−83.73	−87.83
Angular offset (40%)	−85.94	−81.74	−84.11

3.1.2. Voltage FFT Analysis

The phase voltage spectrum is expected to show higher harmonic content than that of the stator current, especially for the third and ninth harmonics. As shown in Table 4 and Figure 6, the voltage FFT reveals only slight differences between the healthy and eccentric cases, except the angular offset case, which shows a noticeable increase in the seventh and ninth harmonics of approximately 5 dB.

Table 4. Amplitudes of the 3rd, 5th, 7th, and 9th harmonics in the voltage spectrum for each SE type compared to the healthy case.

Case	$3f_s$ (dB)	$5f_s$ (dB)	$7f_s$ (dB)	$9f_s$ (dB)
Healthy	−28.97	−82.71	−86.11	−65.38
Axial offset (40%)	−28.89	−83.76	−94.25	−65.63
Radial offset (1.64 mm)	−29.15	−84.48	−93.11	−68.32
Angular offset (40%)	−28.87	−83.86	−80.37	−60.43

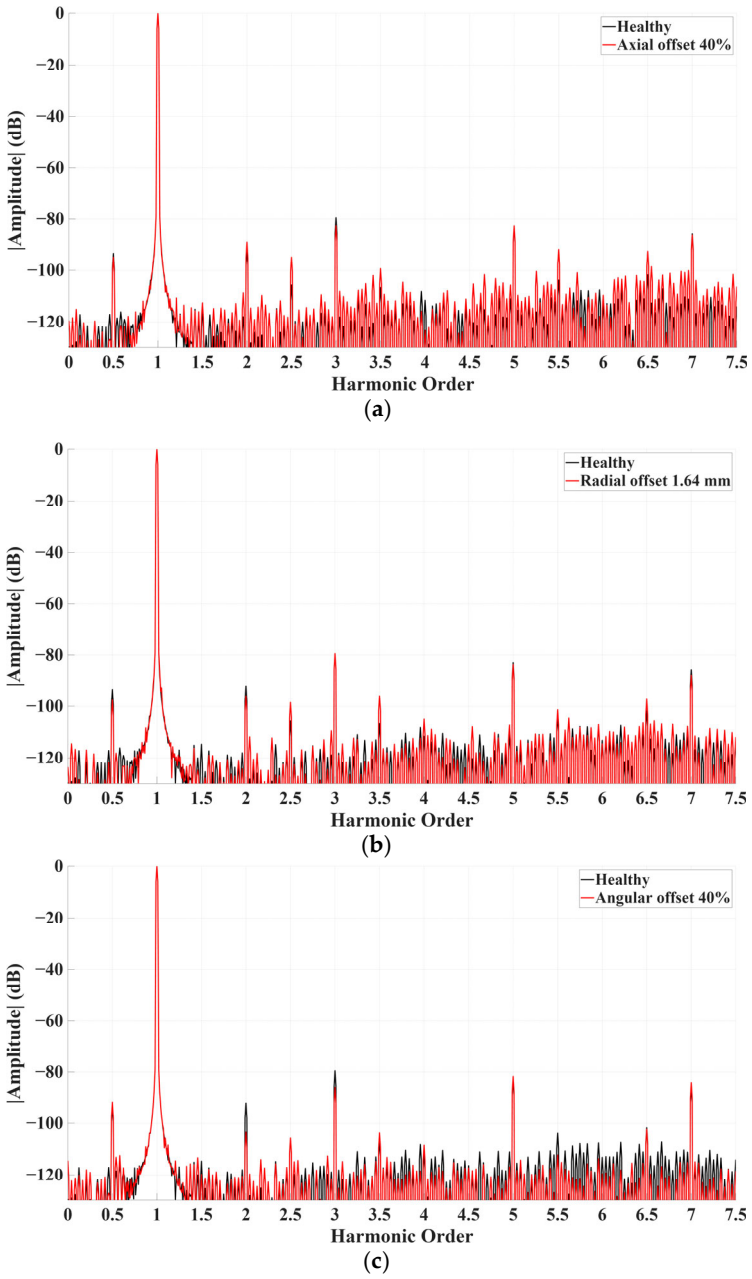

Figure 5. Frequency spectrum of the stator current comparing the healthy case (black) with each SE configuration (red): (**a**) axial offset case with 40% severity, (**b**) radial offset case with 1.64 mm displacement, and (**c**) angular offset case with 40% severity.

3.1.3. Electromagnetic Torque Analysis

The electromagnetic torque is considered a valuable diagnostic tool as it is influenced by both the current and voltage. First, the torque is evaluated in the time domain in order to observe the steady-state behavior and the overall impact of each SE topology. As can be seen from Figure 7, the axial offset case shows a slight increase in the average torque, while the radial displacement fault leads to a noticeable reduction. Meanwhile, the angular offset case follows the healthy torque signal.

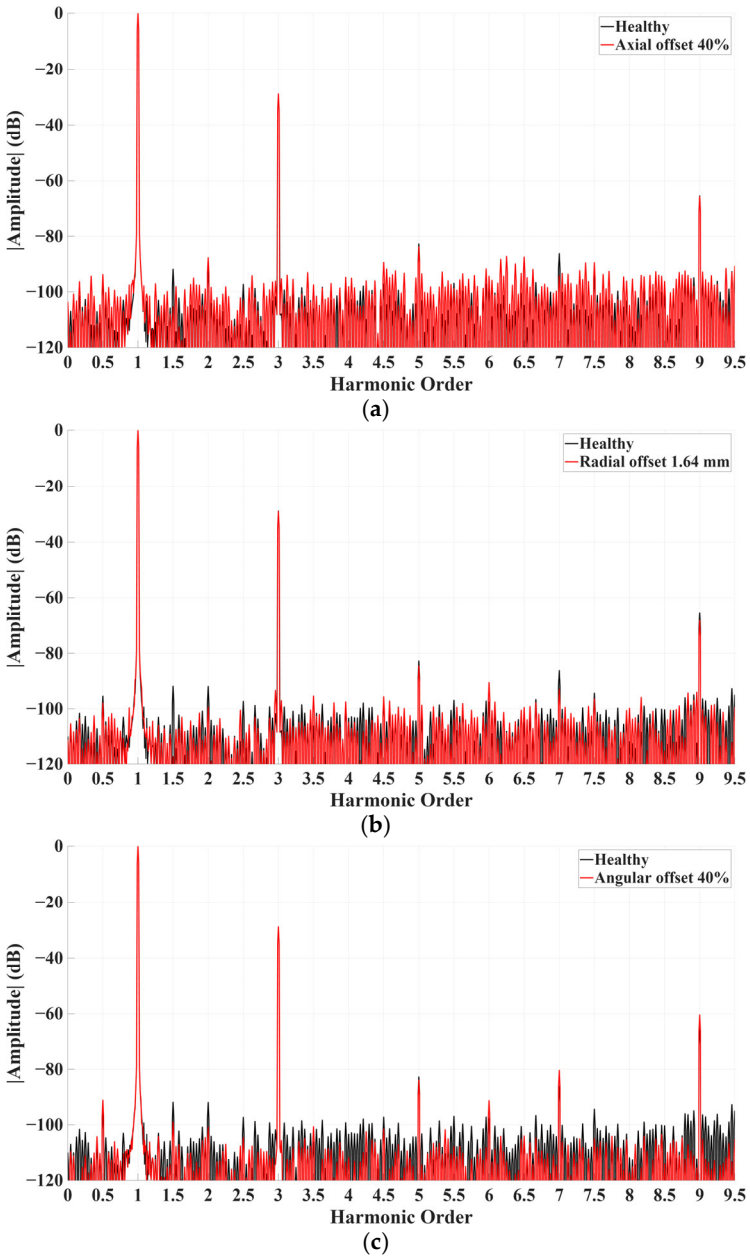

Figure 6. Frequency spectrum of the phase voltage comparing the healthy case (black) with each SE configuration (red): (**a**) axial offset case with 40% severity, (**b**) radial offset case with 1.64 mm displacement, and (**c**) angular offset case with 40% severity.

The harmonic content of the torque spectrum is relevant to the spectral characteristics of the current and voltage signals. Since the presence of SE in this machine cannot be detected with accuracy by using these signals, the torque spectrum will also not produce any noticeable pattern. In the presence of a static eccentricity fault, the magnetic field distribution becomes asymmetrical, which changes the interaction between the rotor and the stator magnetic fields. For that reason, the asymmetry amplifies the second and fourth harmonics, which appear due to the interaction of the first and third harmonics of the stators alternating magnetic fields with the first harmonic of the rotor. However, as shown in Table 5 and Figure 8, only slightly noticeable differences are present. These observations lead to the conclusion that electromagnetic torque is not a sufficient indicator for detecting SE faults in a dual-rotor PMSG.

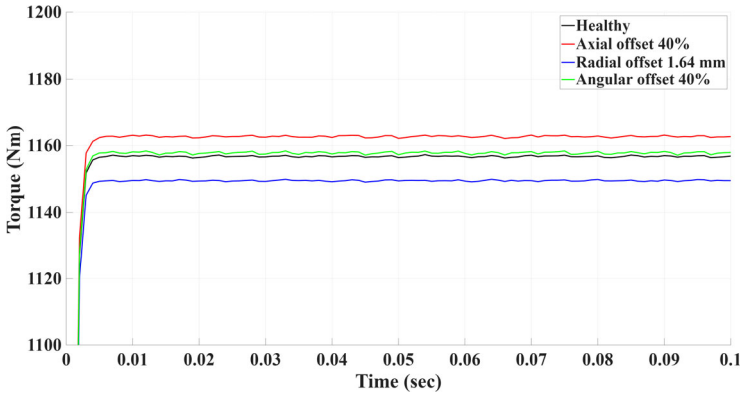

Figure 7. Electromagnetic torque signal of the healthy PMSG (black) and the eccentric PMSGs: axial offset case with 40% severity (red), radial offset case with 1.64 mm displacement (blue), and angular offset case with 40% severity (green).

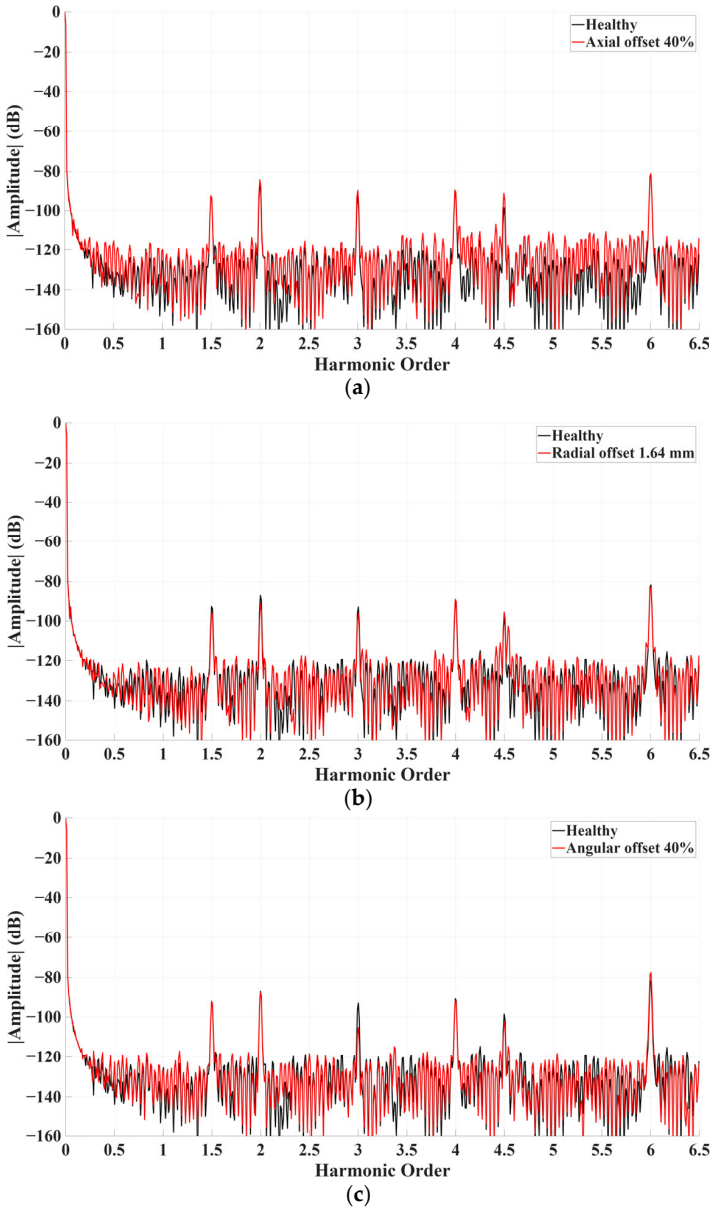

Figure 8. Frequency spectrum of the electromagnetic torque comparing the healthy case (black) with each SE configuration (red): (**a**) axial offset case with 40% severity, (**b**) radial offset case with 1.64 mm displacement, and (**c**) angular offset case with 40% severity.

Table 5. Amplitudes of the 2nd and 4th harmonics in the torque spectrum for each SE type compared to the healthy case.

Case	$2f_s$ (dB)	$4f_s$ (dB)
Healthy	−86.79	−90.88
Axial offset (40%)	−84.08	−89.64
Radial offset (1.64 mm)	−91.26	−89.24
Angular offset (40%)	−87.40	−91.72

3.2. Dynamic Eccentricity

For this study, DE was introduced in the radial and angular offset configurations, both of which inherently generate rotating asymmetries during operation. The axial offset configuration, on the other hand, results in a spatially fixed imbalance and is therefore not considered in the DE analysis. The dynamic nature of this fault is reflected in the appearance of spectral sidebands around the harmonics of the electrical frequency. This occurs because DE introduces a rotating airgap asymmetry that interacts with the spatial magnetic field of the machine. As the rotor revolves, this moving distortion causes periodic variations in the magnetic flux linkage, which is induced by the stator coils. Since each stator coil senses the fault once per mechanical revolution of the rotor, the modulation frequency introduced by the fault is equal to the rotational frequency $f_r = \frac{f_s}{p}$. As a result, the electromagnetic quantities such as current and voltage exhibit sideband components at frequencies of the form $kf_s \pm \frac{f_s}{p}$, where k is an integer.

3.2.1. Current FFT Analysis

The analysis of the current led to the following results, summarized in Table 6 and Figure 9. The sidebands of the third harmonic showed the most notable amplification of the spectral features. Although the sideband amplitudes remained low overall, clear fault-induced amplification was observed. In the radial offset configuration, both sidebands increased, with the right sideband $3f_s + \frac{f_s}{p}$ showing the most significant rise, which is approximately 26 dB higher than the healthy case. On the contrary, the angular offset case produced a moderate spectrum, with the right sideband showing a 10 dB increase. These results confirm that the sideband amplitudes around the third harmonic vary with the type of dynamic eccentricity configuration, with the radial offset case being more detectable.

Table 6. Amplitudes of the sideband harmonics in the current spectrum for each DE type compared to the healthy case.

Case	$3f_s - \frac{f_s}{p}$ (dB)	$3f_s + \frac{f_s}{p}$ (dB)
Healthy	−118.86	−118.11
Radial offset (1.64 mm)	−95.80	−92.97
Angular offset (40%)	−112.13	−108.51

3.2.2. Voltage FFT Analysis

The voltage spectra showcased a similar trend to the current, particularly in the presence of sideband components around the third harmonic, as shown in Table 7 and Figure 10. However, it was observed that in the radial offset case, the third harmonic sidebands experienced greater amplification compared to the current spectrum. Additionally, the angular offset harmonics got diminished, a fact that signifies the existence of a cancelation phenomenon for this case, which is more present in the voltage spectra than in the current.

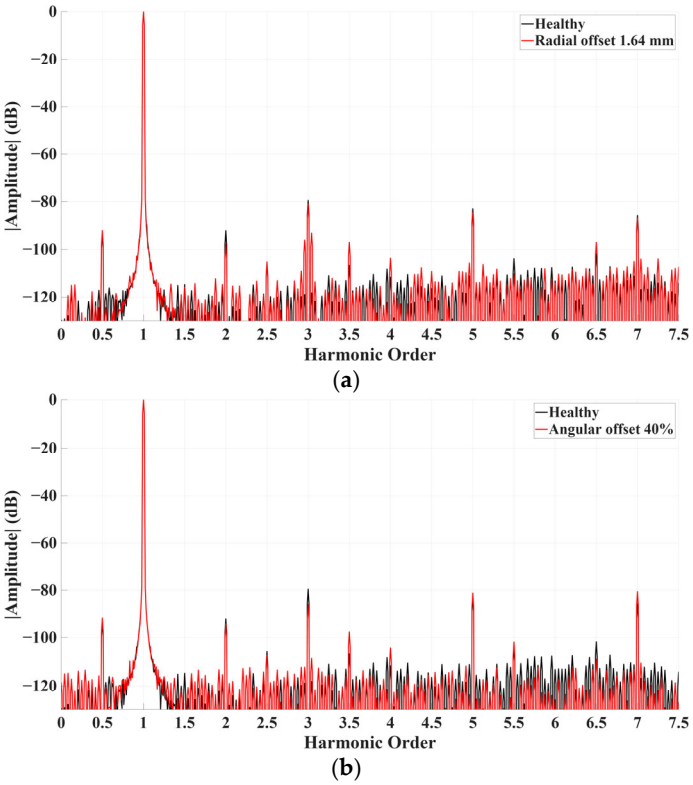

Figure 9. Frequency spectrum of the stator current comparing the healthy case (black) with each DE configuration (red): (**a**) radial offset case with 1.64 mm displacement and (**b**) angular offset case with a 40% ratio.

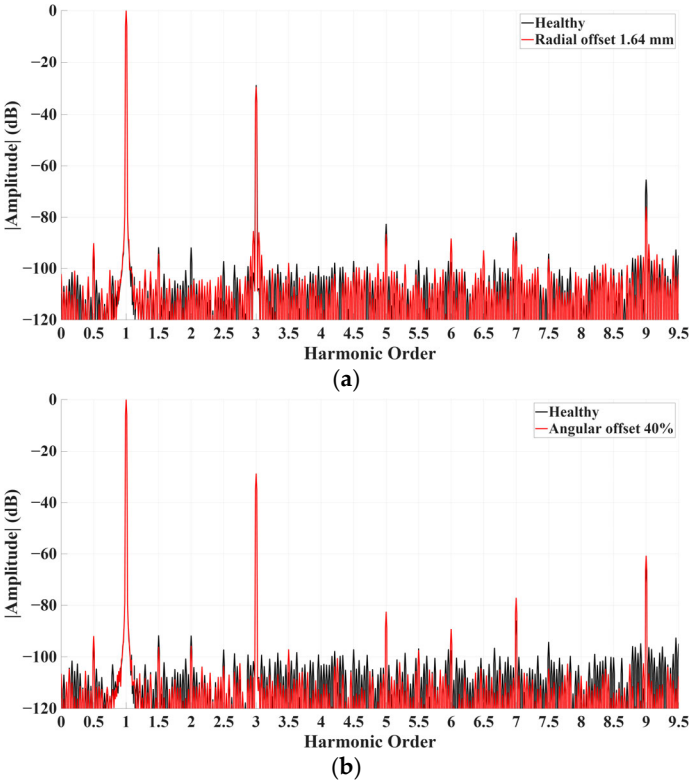

Figure 10. Frequency spectrum of the phase voltage comparing the healthy case (black) with each DE configuration (red): (**a**) radial offset case with 1.64 mm displacement and (**b**) angular offset case with a 40% ratio.

Table 7. Amplitudes of the sideband harmonics in the voltage spectrum for each DE type compared to the healthy case.

Case	$3f_s - \frac{f_s}{p}$ (dB)	$3f_s + \frac{f_s}{p}$ (dB)
Healthy	−101.76	−107.78
Radial offset (1.64 mm)	−85.47	−85.95
Angular offset (40%)	−107.88	−108.22

3.2.3. Electromagnetic Torque Analysis

The electromagnetic torque follows the same pattern as that observed in the SE investigation. In the time-domain analysis, the average torque remains stable with no oscillations. This indicates that the effect of DE on the machine's torque and output power is minimal. In Figure 11, this phenomenon can be seen, while the average torque drop of the angular offset case is present, in a similar way as in the SE investigation.

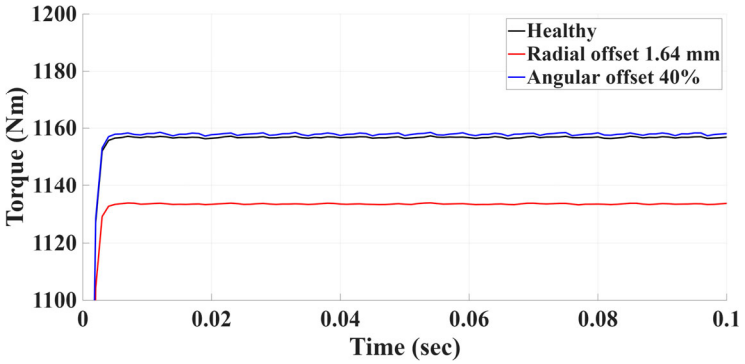

Figure 11. Electromagnetic torque signal of the healthy PMSG (black) and the PMSGs with DE: radial offset case with 1.64 mm displacement (red) and angular offset case with 40% ratio (blue).

The frequency domain analysis of the electromagnetic torque revealed a sensible increase in the second and fourth harmonic sidebands, as expected. In the radial offset case, both harmonics exhibited comparable sideband amplitudes. However, the angular offset configuration showed a more distinct behavior, with the sideband $4f_s + \frac{f_s}{p}$ increasing by approximately 10 dB compared to the healthy case. This phenomenon aligns with the current spectrum results, which confirms the relationship between the electromagnetic torque and the interaction of stator and rotor field harmonics. Specifically, the third harmonic sideband in the stator current ($3f_s + \frac{f_s}{p}$) interacts with the rotor's fundamental harmonic, resulting in an amplified fourth harmonic sideband. Consequently, the fourth torque harmonic exhibits greater sensitivity to the DE faults than the second harmonic, making the angular offset fault more distinguishable. The aforementioned spectral features can be seen in Table 8 and Figure 12.

Table 8. Amplitudes of the sideband harmonics in the torque spectrum for each DE type compared to the healthy case.

Case	$2f_s - \frac{f_s}{p}$ (dB)	$2f_s + \frac{f_s}{p}$ (dB)	$4f_s - \frac{f_s}{p}$ (dB)	$4f_s + \frac{f_s}{p}$ (dB)
Healthy	−120.60	−123.69	−119.49	−122.22
Radial offset (1.64 mm)	−107.71	−101.43	−98.99	−96.24
Angular offset (40%)	−118.86	−116.08	−117.19	−112.06

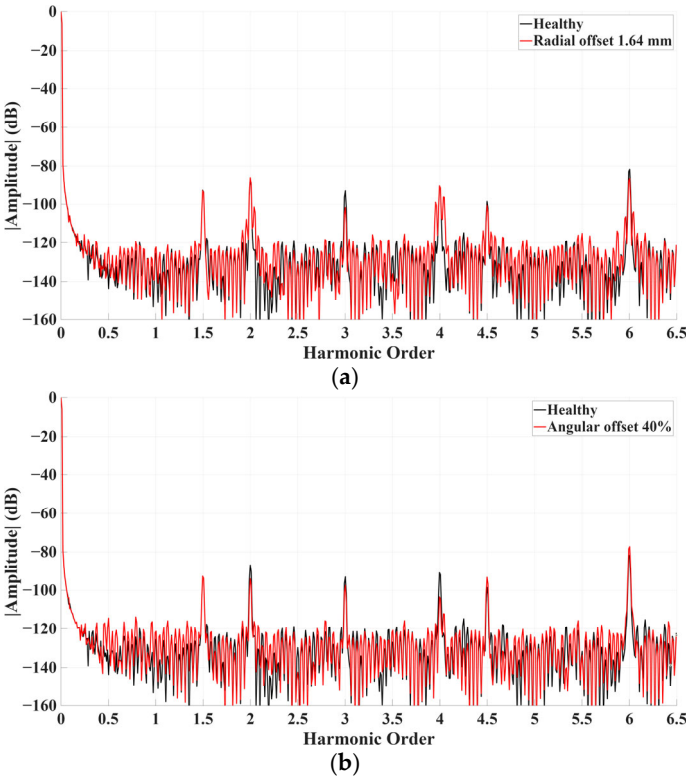

Figure 12. Frequency spectrum of the electromagnetic torque comparing the healthy case (black) with each DE configuration (red): (**a**) radial offset case with 1.64 mm displacement and (**b**) angular offset case with a 40% ratio.

4. Conclusions and Future Work

This study examined the influence of three distinct eccentricity configurations—axial, radial, and angular offset—under both SE and DE conditions in a coreless double-rotor C-GEN PMSG. A 3D FEA model was utilized to study the electromagnetic behavior of the generator, with the investigated features being the stator current FFT, phase voltage FFT, and the electromagnetic torque. In the case of SE, the dual-rotor architecture had the effect of mirroring the asymmetries between the two rotors, which led to a reduction in the expected fault induced signatures. This effect was present in the spectral content of all the investigated quantities, with limited harmonic amplification. An exception was observed in the angular offset case, where the voltage spectrum showed a slight increase in the seventh and ninth harmonics. In the DE study, the radial offset case stood out, as in all spectral features, the sidebands reached a higher than 20 dB difference than the healthy case, with the voltage showing better indications. This difference in the voltage and current spectral responses is a consequence of the unique electromagnetic behavior of the dual-rotor coreless topology, where the voltage reflects back-EMF asymmetries more directly, while the current is influenced by the impedance. The torque analysis showed good indications in the case of DE, which was reflected in the current spectrum. Given these results, particularly the amplification of sidebands by 20 dB in the radial offset configuration, a spectral deviation of 15–20 dB from the healthy case could be considered suitable for early fault detection in similar coreless dual-rotor machines. The comparison between the investigated electromagnetic features can be seen in Table 9.

Table 9. Comparative analysis of the studied electromagnetic features under eccentricity faults.

Feature Type	Observations	SE Detection Capability	DE Detection Capability	Notes
Stator Current FFT	Sidebands at $3f_s + \frac{f_s}{p}$ (DE only)	Low (mirroring effect cancels signatures)	Moderate (sidebands observed, especially in radial offset)	Difficult to detect SE due to double-rotor topology.
Phase Voltage FFT	Harmonics in $7f_s$ and $9f_s$ (SE), Sidebands in $3f_s + \frac{f_s}{p}$ (DE)	Low-Moderate (angular offset detectable)	Moderate (more amplification in radial offset case)	Low amplitudes of the harmonic components
Torque FFT and Time	Sideband of 4th harmonic: $4f_s + \frac{f_s}{p}$ (DE)	Low (no oscillation or harmonic signatures)	Moderate (clear in radial DE case)	Torque spectrum behavior correlates with the current.

It is important to emphasize that harmonic components alone are not sufficiently sound indicators for reliable fault detection and identification. This limitation arises not only from the inherently low amplitudes of the spectral components but also from the fact that factors such as design parameters, load conditions, winding configurations, and manufacturing tolerances can influence the harmonic content significantly. Hence, the focus of future research should be on the reliability enhancement of the fault identification in coreless double-rotor axial PMSGs, using advanced data-driven techniques and AI-based methods to classify the low-amplitude fault harmonics and the harmonics generated due to different operational factors that are not fault-related. Additionally, the use of stray flux sensors is investigated, as flux signals capture electromagnetic asymmetries more directly, regardless of the circuit configurations. By placing three sensors spaced 120 electrical or mechanical degrees apart, the resulting zero-sequence signal would amplify fault signatures and potentially improve the diagnostic outcome. Future work will also focus on the analysis of more complex eccentricity configurations, such as combined radial–axial and radial–angular offsets. Additionally, the impact of mixed eccentricity on the electromagnetic spectra will be explored in order to assess the fault indication capabilities in more severe cases with the appearance of both dynamic and static spectral components.

Author Contributions: Conceptualization, M.S. and K.N.G.; methodology, M.S., A.S. and K.N.G.; software, M.S. and A.S.; validation, M.S., A.S. and K.N.G.; formal analysis, K.N.G.; investigation, M.S. and K.N.G.; resources, M.S. and M.M.; writing—original draft preparation, M.S. and K.N.G.; visualization, M.S.; supervision, M.M. and K.N.G.; project administration, M.M.; funding acquisition, M.M. and K.N.G. All authors have read and agreed to the published version of the manuscript.

Funding: This work has been supported by the EU HORIZON and UKRI project entitled "MEGA PTO WAVE", EU HORIZON project ID: 101147321 https://www.megawave-pto.eu/ (accessed on 19 February 2026).

Data Availability Statement: The original contributions presented in this study are included in the article. Further inquiries can be directed to the corresponding author.

Conflicts of Interest: The authors declare no conflicts of interest.

References

1. Nguyen, P.T.H.; Stüdli, S.; Braslavsky, J.H.; Middleton, R.H. Lyapunov Stability of Grid-Connected Wind Turbines with Permanent Magnet Synchronous Generator. *Eur. J. Control* **2022**, *65*, 100615. [CrossRef]
2. Freire, N.M.A.; Cardoso, A.J.M. Fault Detection and Condition Monitoring of PMSGs in Offshore Wind Turbines. *Machines* **2021**, *9*, 260. [CrossRef]
3. Keysan, O.; Mueller, M.; McDonald, A.; Hodgins, N.; Shek, J. Designing the C-GEN Lightweight Direct Drive Generator for Wave and Tidal Energy. *IET Renew. Power Gener.* **2012**, *6*, 161–170. [CrossRef]

4. Zhao, J.; Ma, T.; Liu, X.; Zhao, G.; Dong, N. Performance Analysis of a Coreless Axial-Flux PMSM by an Improved Magnetic Equivalent Circuit Model. *IEEE Trans. Energy Convers.* **2021**, *36*, 2120–2130. [CrossRef]
5. Singh, K.A.; Chaudhary, A.; Chaudhary, K. Three-Phase AC-DC Converter for Direct-Drive PMSG-Based Wind Energy Conversion System. *J. Mod. Power Syst. Clean Energy* **2023**, *11*, 589–598. [CrossRef]
6. Mudigonda, B.; Moretti, G.; Tedeschi, E. An Overview of Permanent Magnet Generator Architectures and Control for Wave Energy Conversion Systems. *Energies* **2026**, *19*, 134. [CrossRef]
7. Barmpatza, A.C.; Kappatou, J.C.; Skarmoutsos, G.A. Investigation of Static Angular and Axis Misalignment in an AFPM Generator. In Proceedings of the 2019 IEEE Workshop on Electrical Machines Design, Control and Diagnosis (WEMDCD), Athens, Greece, 22–23 April 2019; Volume 1, pp. 163–168.
8. Koura, M.B.; Boudinar, A.H.; Aimer, A.F.; Bendiabdellah, A.; Gherabi, Z. Diagnosis and Discernment between Eccentricity and Demagnetization Faults in PMSM Drives. *J. Power Electron.* **2021**, *21*, 563–573. [CrossRef]
9. Okazaki, K.; Akatsu, K.; Yang, K. Detection Method of Static Eccentricity Using Third-Order Harmonic Component of No-Load Line-Line Voltages on Three-Group and Three-Phase Permanent Magnet Synchronous Motors. In Proceedings of the 2021 IEEE International Electric Machines & Drives Conference (IEMDC), Hartford, CT, USA, 17–20 May 2021; pp. 1–6.
10. Kim, Y.-S.; Yang, J.-W.; Kim, Y.-J.; Shin, K.-H.; Choi, J.-Y. Analytical and Experimental Approaches to Predicting Magnetic Field Asymmetry and Electromagnetic Forces in Slotted Surface-Mounted Permanent Magnet Machines with Rotor Eccentricity. *IEEE Trans. Magn.* **2025**, *61*, 8102605. [CrossRef]
11. Du, Y.; Wu, L.; Zhan, H.; Ruan, G.; Fang, Y. Investigation of Postdemagnetization Unbalanced Magnetic Force in PM Machines Considering Short-Circuit Faults. *IEEE Trans. Transp. Electrif.* **2021**, *7*, 2728–2742. [CrossRef]
12. Mirimani, S.M.; Vahedi, A.; Marignetti, F. Effect of Inclined Static Eccentricity Fault in Single Stator-Single Rotor Axial Flux Permanent Magnet Machines. *IEEE Trans. Magn.* **2012**, *48*, 143–149. [CrossRef]
13. Ebrahimi, B.M.; Faiz, J.; Roshtkhari, M.J. Static-, Dynamic-, and Mixed-Eccentricity Fault Diagnoses in Permanent-Magnet Synchronous Motors. *IEEE Trans. Ind. Electron.* **2009**, *56*, 4727–4739. [CrossRef]
14. Haddad, R.Z.; Strangas, E.G. On the Accuracy of Fault Detection and Separation in Permanent Magnet Synchronous Machines Using MCSA/MVSA and LDA. *IEEE Trans. Energy Convers.* **2016**, *31*, 924–934. [CrossRef]
15. Sergakis, A.; Salinas, M.; Gkiolekas, N.; Gyftakis, K.N. A Review of Condition Monitoring of Permanent Magnet Synchronous Machines: Techniques, Challenges and Future Directions. *Energies* **2025**, *18*, 1177. [CrossRef]
16. Ogidi, O.O.; Barendse, P.S.; Khan, M.A. Detection of Static Eccentricities in Axial-Flux Permanent-Magnet Machines with Concentrated Windings Using Vibration Analysis. *IEEE Trans. Ind. Appl.* **2015**, *51*, 4425–4434. [CrossRef]
17. Wang, Z.; Shi, S.; Gu, X.; Xu, Z.; Wang, H.; Zhang, Z. Fault Diagnosis Method of Permanent Magnet Synchronous Motor Demagnetization and Eccentricity Based on Branch Current. *World Electr. Veh. J.* **2025**, *16*, 223. [CrossRef]
18. Ebrahimi, B.M.; Javan Roshtkhari, M.; Faiz, J.; Khatami, S.V. Advanced Eccentricity Fault Recognition in Permanent Magnet Synchronous Motors Using Stator Current Signature Analysis. *IEEE Trans. Ind. Electron.* **2014**, *61*, 2041–2052. [CrossRef]
19. Yu, Y.; Gao, H.; Zhou, S.; Pan, Y.; Zhang, K.; Liu, P.; Yang, H.; Zhao, Z.; Madyira, D.M. Rotor Faults Diagnosis in PMSMs Based on Branch Current Analysis and Machine Learning. *Actuators* **2023**, *12*, 145. [CrossRef]
20. Safa, H.H.; Ebrahimi, M.; Zarchi, H.A.; Abshari, M. Eccentricity Fault Detection in Permanent Magnet Synchronous Generators Using Stator Voltage Signature Analysis. *Int. J. Precis. Eng. Manuf.* **2017**, *18*, 1731–1737. [CrossRef]
21. López-Torres, C.; Riba, J.-R.; Garcia, A.; Romeral, L. Detection of Eccentricity Faults in Five-Phase Ferrite-PM Assisted Synchronous Reluctance Machines. *Appl. Sci.* **2017**, *7*, 565. [CrossRef]
22. Barmpatza, A.C. The Neutral Voltage Difference Signal as a Means of Investigating Eccentricity and Demagnetization Faults in an AFPM Synchronous Generator. *Machines* **2023**, *11*, 647. [CrossRef]
23. Jung, W.-S.; Kim, Y.-S.; Choi, Y.-T.; Shin, K.-H.; Choi, J.-Y. Electromagnetic and NVH Characteristic Analysis of Eccentric State for Surface-Mounted Permanent Magnet Synchronous Generators in Wave Power Applications. *Appl. Sci.* **2025**, *15*, 9697. [CrossRef]
24. Ogidi, O.O.; Barendse, P.S.; Khan, M.A. Influence of Rotor Topologies and Cogging Torque Minimization Techniques in the Detection of Static Eccentricities in Axial-Flux Permanent-Magnet Machine. *IEEE Trans. Ind. Appl.* **2017**, *53*, 161–170. [CrossRef]
25. Sergakis, A.; Gkiolekas, N.; Mueller, M.; Gyftakis, K.N. Analysis and Diagnosis of Inter-Turn Short Circuit Faults in Dual Rotor Air-Cored PMSG-Series Connected Stator Coils. In Proceedings of the 2025 IEEE Symposium on Diagnostics for Electric Machines, Power Electronics and Drives (SDEMPED), Dallas, TX, USA, 24–27 August 2025; pp. 1–7.
26. Liu, Z.; Zhang, P.; He, S.; Huang, J. A Review of Modeling and Diagnostic Techniques for Eccentricity Fault in Electric Machines. *Energies* **2021**, *14*, 4296. [CrossRef]
27. Mirimani, S.M.; Vahedi, A.; Marignetti, F.; Di Stefano, R. An Online Method for Static Eccentricity Fault Detection in Axial Flux Machines. *IEEE Trans. Ind. Electron.* **2015**, *62*, 1931–1942. [CrossRef]

28. Karampas, S.; Skarmoutsos, G.; Mueller, M.; Gyftakis, K. Novel Online Static Eccentricity Detection and Evaluation in Permanent Magnet Generators. In Proceedings of the 2024 IEEE Energy Conversion Congress and Exposition (ECCE), Phoenix, AZ, USA, 20–24 October 2024; pp. 5788–5793.
29. Zhu, G.; Luo, J. Unbalanced Magnetic Pull Calculation in Ironless Axial Flux Motors. *Energies* **2025**, *18*, 2397. [CrossRef]